Carrier dynamics in microcrystalline silicon studied by time-resolved terahertz spectroscopy

L. Fekete, H. Němec, F. Kadlec, P. Kužel *, J. Stuchlík, A. Fejfar, J. Kočka

Institute of Physics, Academy of Sciences of the Czech Republic, Na Slovance 2, 182 21 Prague 8, Czech Republic

Abstract

We present results of optical pump – terahertz probe experiments applied to a set of thin film silicon samples on sapphire substrates. Structure of the films varied from amorphous to fully microcrystalline. Picosecond time scale evolution of electrical transport properties of photoexcited samples is investigated and discussed. Three different mechanisms are found to contribute to the dynamical conductivity at terahertz frequencies.
© 2006 Elsevier B.V. All rights reserved.

1. Introduction

Microcrystalline silicon (µc-Si:H) has attracted considerable attention during the last years for use in photovoltaic applications, as well as active matrix displays and other opto-electronic elements [1]. This is due to the fact that it combines the opto-electronic properties of crystalline silicon with those of low-cost thin-film technology. Indeed, silicon can be grown on cheap substrates, like glass or plastic materials, by various deposition methods including PECVD and hot-wire deposition. The improvement of efficiency of the layers suited for applications is critically dependent on the detailed knowledge of charge carrier dynamics. The deposition conditions of the thin films allow for the tuning of such film characteristics as grain size, their arrangement and degree of crystallinity, which are expected to influence strongly the lifetime and mobility of carriers.

The time-domain terahertz (THz) spectroscopy is a contact-free method highly sensitive to mobile charges, and, consequently well suited for the dynamical investigation of photo-excited semiconductors [2,3]. In this contribution we report on optical pump – THz probe (OPTP) experiments for a series of 1 µm-thick µc-Si:H layers with a variable crystallinity deposited on sapphire substrates. The experiment allows one to obtain broadband transient THz spectra of the films as a function of the pump–probe delay and, subsequently, to identify different contributing mechanisms.

2. Experimental

All samples were prepared by plasma-enhanced chemical vapor deposition (PECVD) at 250 °C and 70 Pa. The deposition parameters were adjusted to obtain samples with different degree of crystallinity from amorphous sample to a highly microcrystalline one. The sample thicknesses were determined by surface profile measuring. Crystallinity of the samples was determined from the integrated

---

contributions of the amorphous and crystalline components found by decomposition of the Raman scattering spectra excited by Ar^+ and He–Ne lasers (wavelengths 514 and 633 nm, respectively), taking into account the ratio of back scattering cross sections of the phases [4]. The light penetration depth in microcrystalline silicon for 514 nm excitation is about 0.25 μm: the Raman spectra thus provide information on the crystallinity close to the film surface which is usually higher than that close to the substrate. The penetration depth for the light at 633 nm is of about 1.5 μm: the experiment at this wavelength yields an average crystallinity degree over the whole sample thickness. The sample characteristics are summarized in Table 1. The sample a-C0 is fully amorphous, the remaining ones contain the microcrystalline phase. As substrates, $1\bar{1}02$-oriented $10 \times 5 \times 0.5$ mm^3 sapphire plates, transparent for both THz and optical radiation, were used.

For the THz time-domain experiments we used an experimental scheme similar to that described in [3]. Ti:sapphire multipass amplifier was used as a femtosecond laser source and the laser pulses were split into three branches, all of them including delay lines for precise control of pulse arrival times. The first (pump) branch of the laser beam was used for optical excitation of the sample. The second (probe) branch was used for generating THz radiation in a 1 mm thick [011] ZnTe crystal via optical rectification (probe branch). The radiation was focused onto the sample using an ellipsoidal mirror such that the THz beam size was smaller than that of the optical pump beam to ensure a homogeneous excitation. The last (sampling) branch served for an electro-optic detection of the transmitted THz electric field using another [011] ZnTe crystal [5]. The principal axes of the birefringent substrates were carefully aligned with the THz beam polarization using a pair of crossed wire-grid polarizers.

A synchronous detection scheme used was locked to a mechanical chopper at 166 Hz placed either in the pump or probe branch. Let $E(\tau)$ be a time profile of the electric field transmitted through the sample in equilibrium, i.e., when the pump beam is blocked and the chopper is placed into the probe branch (τ, represents the real time; in the experiment it is connected to the delay of the sampling pulse). If the chopper is moved into the pump branch, pump-induced changes in the THz waveform $\Delta E(\tau,\tau_p)$ can be directly measured (τ_p is the pump–probe time delay). Two different types of experiments were performed for all the samples:

(i) Pump–probe scans where τ was fixed at the maximum of the transient waveform $\Delta E_{max}(\tau,\tau_p)$ and τ_p was varied (see Fig. 1).
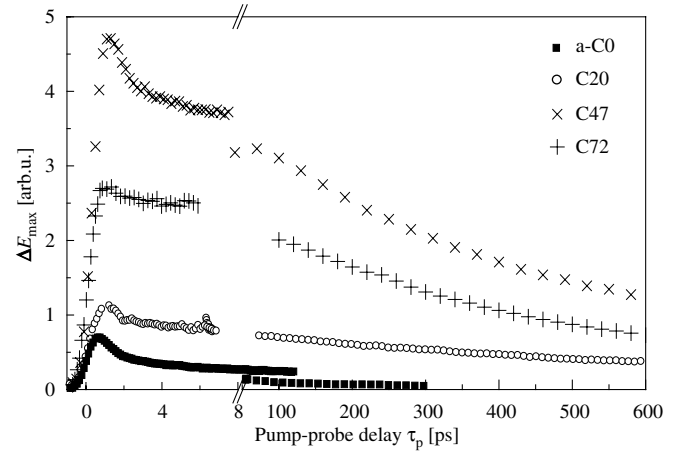

Fig. 1. Pump–probe scans: maximum field amplitude of the transient THz signal (ΔE_{max}) versus pump–probe delay.
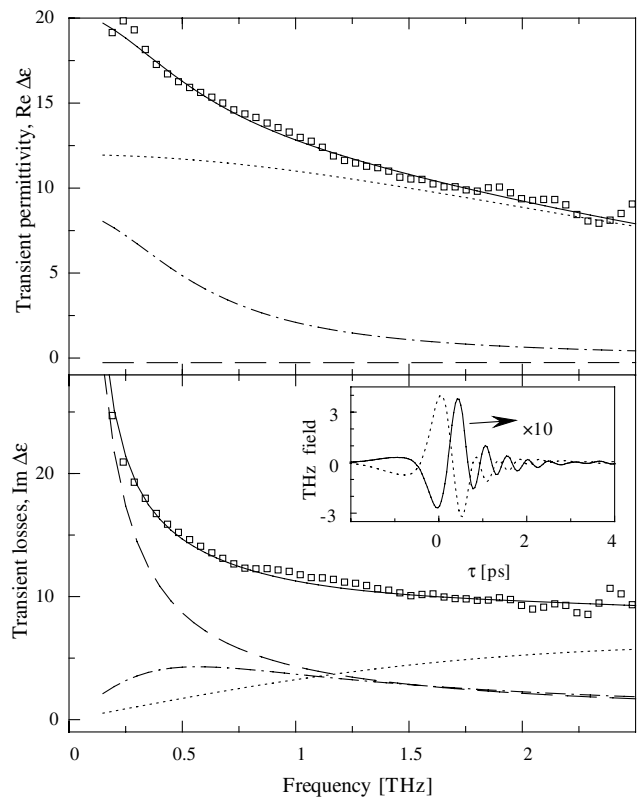

Fig. 2. Transient dielectric spectra of C72 μc-Si:H sample for $\tau_p = 150$ ps. Experimental data are represented by symbols (their error is smaller than 5%). The solid line corresponds to the best fit of Eq. (4) to the data (see the text for details). The decomposition of the fit into individual contributions is also shown: Drude term (dashed line), slow relaxator (dash-dotted line), fast relaxator (dotted line). Inset: time-domain waveforms (raw data); dotted line: equilibrium (reference) waveform $E(\tau)$, full line: transient waveform $\Delta E(\tau,\tau_p)$.

Table 1
Characteristics of the samples

Sample code	C_{633nm} [%]	C_{514nm} [%]	Thickness [nm]	RF power [W]	H_2/SiH_4
a-C0	0	0	890 ± 50	9.5	12.8
C20	20	59	920 ± 50	9.5	23.8
C47	47	71	770 ± 50	9.5	29.4
C72	72	73	770 ± 50	9.7	47.6

(ii) Measurements of transient waveforms $\Delta E(\tau, \tau_p)$ with fixed values of τ_p (equal to 11, 26, 56, 150, 300, and 600 ps): see an example in Fig. 2. Transient THz transmission spectra can be calculated from the Fourier transform of the signals using the relation $\Delta T(\omega, \tau_p) = \Delta E(\omega, \tau_p)/E(\omega)$. Instantaneous spectral snapshots of the complex photoconductivity $\Delta\sigma(\omega, \tau_p)$ – or equivalently of the complex permittivity $\Delta\varepsilon(\omega, \tau_p)$ (where $\Delta\sigma = i\omega\varepsilon_0\Delta\varepsilon$) – then can be determined from the experimental data.

3. Results

THz probing radiation strongly interacts with mobile charges. Photoexcited electrons in amorphous or microcrystalline silicon are characterized by a delocalized wave function (free carriers participating in the DC conductivity): such carriers can be probed by THz pulses if their plasma frequency falls into or exceeds the THz range. Subsequently, the free carriers can be captured into deep or shallow levels or they can be constrained by potential barriers at grain boundaries: their motion is then described by a localized wave function and they can be detected by the THz radiation if their resonant frequency lies in the THz range and if they remain mobile. The transient THz response thus may involve several contributions showing quite different spectral characteristics.

The THz pump–probe scans of $\Delta E_{max}(\tau, \tau_p)$ show an overall dynamics of the system averaged over all possible contributions. We can identify in Fig. 1 a fast (2 ps) component which was previously observed and attributed to the carrier trapping into deep saturable levels [6]. In this paper we focus on the slow decay which extends typically over hundreds of ps for our samples. Fig. 1 clearly shows that this slow component strongly depends on the crystallinity of samples. (i) We observe a significant increase of the amplitude of the slow component for microcrystalline samples as compared to the amorphous one. (ii) In agreement with optical pump–optical probe measurements [7] the amorphous sample exhibits a bimolecular recombination (hyperbolic decay) while in the microcrystalline samples the decay is exponential and significantly slower.

As mentioned above, the OPTP technique allows us to determine broadband transient THz spectra for each pump–probe delay. We have experimentally determined such transient THz spectra at $\tau_p = 11$, 26, 56, 150, 300 and 600 ps for each sample studied. An example is shown in Fig. 2.

4. Discussion

The set of experimentally obtained transient THz spectra allows us to identify individual components corresponding to different conductivity mechanisms. Generalizing our results presented in Ref. [3] the dynamical dielectric response of our samples reads:

$$\Delta\varepsilon(\omega, \tau_p) = \sum_i n_i(\tau_p)f_i(\omega), \qquad (1)$$

where we sum over individual contributions to the THz response; $n_i(\tau_p)$ describes the carrier density decay for the i-th component and $f_i(\omega)$ is the corresponding spectral response. We emphasize that the response function (1) can be factorized only for a sufficiently slow signal decay (i.e., it should well exceed the THz pulse length and the characteristic time of the spectral response) which is fulfilled in the present case. We use the following models for the spectral response:

(i) Free carrier dynamics is described by the Drude model:

$$f_D(\omega) = -\frac{1}{i\omega(1 - i\omega\tau_D)}. \qquad (2)$$

The microscopic mobility of microcrystalline samples is known to be much lower than that of Si single crystals: $\mu \leqslant 50$ cm^2/Vs [8]. The corresponding effective momentum scattering time τ_D is of the order of units of fs and does not contribute significantly to the THz spectra: in our fits we assume $\tau_D \lesssim 10$ fs.

(ii) Localized carrier dynamics is expected to be overdamped. To simplify the analysis we model this case by a Debye relaxator with a single relaxation frequency $1/\tau_R$:

$$f_R(\omega) = \frac{1}{1 - i\omega\tau_R}. \qquad (3)$$

Brief inspection of the results presented in Fig. 2 unambiguously shows that both types of contributions are needed to explain for the observed spectra. The low-frequency part of Im $\Delta\varepsilon$ must be described by the Drude term and the positive values of Re $\Delta\varepsilon$ require a significant contribution of localized carriers. A detailed analysis of the whole set of data (several pump–probe delays, all the samples) shows that an interplay of 3 general terms is necessary to account for all the features observed in the spectra:

$$\Delta\varepsilon(\omega, \tau_p) = n_D(\tau_p)f_D(\omega) + n_{R,slow}(\tau_p)f_{R,slow}(\omega)$$
$$+ n_{R,fast}(\tau_p)f_{R,fast}(\omega). \qquad (4)$$

For each sample the complete set of data (involving complex transient spectra for six pump–probe delays) is simultaneously fitted by Eq. (4) using the nonlinear least square method. An example of one particular spectrum along with the fitting curve and its spectral decomposition into individual components is shown in the Fig. 2. The results of all the fits are summarized in Table 2. The carrier densities were found to undergo an exponential decay for microcrystalline samples and a hyperbolic one for the amorphous sample.

One of the major results of our study is the presence of the fast relaxator and the strong dependence of its relaxa-

Table 2
Summary of the spectroscopic results

Sample	Pump–probe decay of n_i			$\tau_{R,fast}$ [fs]	$\tau_{R,slow}$ [fs]
	Drude term [ps]	Fast relax. [ps]	Slow relax. [ps]		
a-C0	60 ± 10	–	50 ± 10	–	310 ± 50
C20	350 ± 50	530 ± 100	>5000	20 ± 10	210 ± 50
C47	380 ± 20	380 ± 20	>5000	55 ± 20	250 ± 50
C72	390 ± 20	390 ± 20	>5000	60 ± 20	220 ± 50

tion time on the crystallinity. On one hand, this relaxator was not observed for the fully amorphous sample, on the other hand, its characteristic time τ_R significantly increases with increasing crystallinity. At the same time, the pump-probe decay of $n_{R,fast}$ is very similar to that of the Drude term. These findings suggest that the underlying microscopic process is linked to the existence (and probably also to the size) of the crystalline grains and that it involves carriers in the conduction band. It then may be related to the confinement of the carriers into individual grains and/or to their pinning to the barriers at the boundaries.

In contrast, the relaxation time of the slow relaxator is practically sample independent and its lifetime exceeds several nanoseconds for microcrystalline samples. It is likely that the mechanism of this process is similar for all the samples. We tentatively attribute it to the motion of trapped carriers in the shallow band tail levels.

5. Conclusion

We have shown that time-resolved THz spectroscopy is able to provide pertinent spectral information on the charge carrier dynamics in microcrystalline and amorphous silicon. We have obtained time-dependent THz spectra of photoexcited samples with different degrees of crystallinity and identified three different contributions of photocarriers to the conductivity. Possible interpretations of these contributions were discussed. Further experiments are in progress which are expected to provide deeper insight into the observed processes.

References

[1] A. Shah, P. Torres, R. Tscharner, N. Wyrsch, H. Keppner, Science 285 (1999) 692.
[2] C.A. Schmuttenmaer, Chem. Rev. 104 (2004) 1759.
[3] H. Němec, F. Kadlec, C. Kadlec, P. Kužel, P. Jungwirth, J. Chem. Phys. 122 (2005) 104504.
[4] R. Tsu, J. Gonzalez-Hernandez, S.S. Chao, S.C. Lee, K. Tanaka, Appl. Phys. Lett. 40 (1982) 534.
[5] A. Nahata, A.S. Weling, T.F. Heinz, Appl. Phys. Lett. 69 (1996) 2321.
[6] P.U. Jepsen, W. Schairer, I.H. Libon, U. Lemmer, N.E. Hecker, M. Birkholz, K. Lips, M. Schall, Appl. Phys. Lett. 79 (2001) 1291.
[7] J. Kudrna, P. Malý, F. Trojánek, J. Štěpánek, T. Lechner, I. Pelant, J. Meier, U. Kroll, Mat. Sci. Eng. B 69&70 (2000) 238.
[8] S. Brehme, P. Kanschat, K. Lips, I. Sieber, W. Fuhs, Mat. Sci. Eng. B 69&70 (2000) 232.